Combined Quantum Mechanics: Interatomic Potential Function Investigation of rac-meso Configurational Stability and Rotational Transition in Zirconocene-Based Ziegler−Natta Catalysts

Amitesh Maiti,*,† Marek Sierka,‡ Jan Andzelm,† Joe Golab,§ and Joachim Sauer‡

Molecular Simulations Inc., 9685 Scranton Road, San Diego, California 92121, BPAmoco Naperville Complex, 150 West Warrenville Road, Naperville, Illinois 60563, and Humboldt-Universität zu Berlin, Institut für Chemie, Arbeitsgruppe Quantenchemie, Jägerstrasse 10−11, D-10117 Berlin, Germany

Received: June 7, 2000; In Final Form: September 6, 2000

The relative energetic stability of the "rac" and the "meso" rotational isomers of metallocene-based Ziegler−Natta (ZN) catalysts plays an important role in determining the structural, physical and chemical properties of synthesized polymers. Due to the large molecular size of these systems, ab initio calculations are often prohibitive. To circumvent this problem, we use the QM-Pot approach, which treats the metal center and its surrounding atoms/ligands by quantum mechanics (QM), whereas the (organic) atoms/functional groups away from the metal center are described by an interatomic potential function (Pot). As a concrete example, we choose a commercially important zirconocene-based catalyst and compute: (1) the relative energies of the rac and meso structures; (2) the activation barrier for the rotational transition from one to the other; and (3) the effect of the addition of organic functional groups on the above energies. Due to small mismatches between QM and Pot potential surfaces, one has to be careful in defining the QM cluster. In particular, larger QM clusters do not necessarily yield better results. Despite these difficulties, we show that it is possible to define a cluster for which the hybrid approach yields meaningful results when compared to full QM calculations.

1. Introduction

Alkene polymerization is one of the most important catalytic reactions in commercial use. Metallocene-based Ziegler−Natta (ZN) catalysts are used to produce some fifteen million tons of polyethylene and polypropylene every year. Even more than forty years after Ziegler's original discovery of the "Aufbau-reaktion" and low-pressure ethene polymerization, metallocene-catalyzed olefin and diolefin polymerization continues to represent one of the most active and exciting research areas. Since the 1980s, outstanding scientific innovations and process improvements have revolutionized polyolefin technology and greatly simplified polymerization processes. New stereostructures and new monomers can now be polymerized, including a wide variety of bulky monomers, phenolic compounds, dienes, and cyclo-olefins. Metallocene catalysis offers a promising new way not only to tailor polymer properties but also to produce entirely new polymeric materials.[1,2]

The atomic structure and the geometrical configuration of a metallocene catalyst determine the rate of synthesis, tacticity, molecular weight, and microstructure of the polymer, which in turn affect its physical and chemical properties. As in many areas of molecular and biomolecular chemistry, prediction of structure−activity correlation is of enormous importance and some attempts have already been made, for example in zirconocene catalysis,[3−5] to explain well-designed experiments. In the present study, the system of interest is a zirconocene catalyst that is technologically important to BPAmoco research and that, in its simplest form, can be represented by the formula [2-Phenyl-Indenyl]$_2$ $ZrCl_2$.[6−8] This molecule, hereafter referred to as the *parent* system, can exist in two conformational states, the rac and the meso, as shown in Figures 1(a, b). These are rotational isomers having the same connectivity and differing primarily in the dihedral angle ABCD, as indicated in Figure 1. Experiments have been designed to synthetically modify this basic catalyst by adding functional groups in the 3, 5 and 3′, 5′ positions of the phenyl groups, respectively.[7] In addition, to study polymerization reactions the two Cl ions are replaced respectively by a growing polymer chain and a monomeric unit. The latter adds to the polymer chain through an insertion reaction. The tacticity and other structural properties of the polymer depend strongly on whether the catalyst is in the rac or the meso configuration. Relative stability of these two configurations and structural transformation from one to the other, therefore, play a very important role in determining the properties of the resulting polymer. Understanding the relative stability of these configurations and the structural transformation of one to the other is of great relevance to catalyst design.[6−8]

Theoretical calculations based on interatomic potential functions (Pot), for example force fields, have proved to be an important tool in predicting the relative energetic stability of catalyst conformers. However, to analyze the chemistry of bond breaking/making processes, e.g., as present in olefin binding and insertion reactions, standard force fields are not appropriate. In such a scenario one would like to use a quantum mechanical (QM) method. Unfortunately, many of these catalysts, along with associated polymeric fragments have rather complex structures with a large number of atoms, and first principles QM computation becomes prohibitively expensive. One alternative is the use of combined QM-Pot methods, also known as QM/MM methods, in which the reactive site is treated explicitly by a QM method, while the surrounding environment, which

† Molecular Simulations Inc.
‡ Humboldt-Universität zu Berlin, Institut für Chemie.
§ BPAmoco Naperville Complex.

10.1021/jp002056l CCC: $19.00
Published on Web 10/21/2000

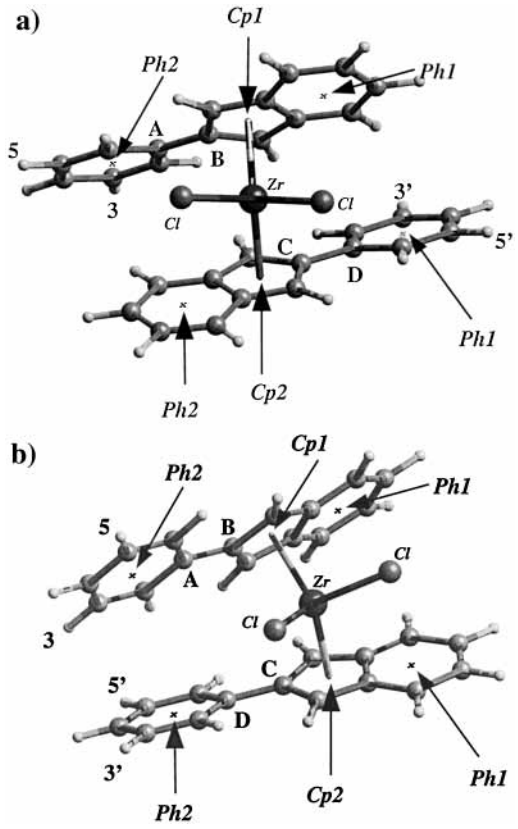

Figure 1. Parent structure in the (a) rac and (b) meso conformations. The tbutyl structure is obtained by attaching *tert*-butyl groups at the (3, 5, 3′, 5′) positions of the phenyl rings. The centers of the cyclopentadiene rings (Cp1, Cp2) and that of the phenyl rings (Ph_1, Ph_2) are used to compute various structural parameters in Tables 1−3. Note that Ph_1 and Ph_2 are defined differently in rac and meso, and the meso-definition is followed in the transition state geometry.

constitutes the most time-consuming part in standard QM calculations, is treated by interatomic potential functions. There is a considerable amount of existing literature on the application of such methods,[9−24] including applications to metallocene catalysts.[22−24] The multitude of applications have used varying formulations of QM/MM methods, differing primarily in two important aspects: (1) how the interactions between the regions treated by the QM and MM methods are defined; and (2) how to treat the boundary region between the interior and the surrounding when there are covalent or partially covalent bonds connecting the two regions.

In this paper we employ the QM-Pot method developed by Sauer and collaborators[9,10] for computing: (1) rac−meso stability; (2) the activation barrier for the rotational transformation from one to the other; and (3) the change in the above energetics as a function of functional group change in the (3, 5, 3′, 5′) positions of the phenyl rings in the parent system (see Figure 1). As a concrete example of an added functional group, we have chosen a relatively large one, i.e., the *tert*-butyl group, which results in a system of more than one hundred atoms. Hereafter, we refer to this large system as the *tbutyl* system.

The main motivation of the present study is to explore (1) the best choice for a QM cluster within the QM-Pot approach for this type of catalyst and (2) the limits of accuracy with the chosen combination of QM method/force field. Due to the lack of experimental data for the energies of interest, comparison is made with results of the QM treatment for the whole system. The lessons learned will guide future QM-Pot studies of polymerization reactions and the variation of the activity and selectivity as a function of the conformation of the catalysts. Full QM treatment will be no longer possible as larger and more complex functional groups may be present and long (and growing) polymer chains as well as incoming monomer units have to be treated. Moreover, as we are dealing here with homogeneous catalysis, a realistic model may require explicit consideration of solvent molecules. This is easily done within QM/MM schemes, see, e.g., refs 20, and 21.

2. Computations

QM-Pot Method. In this paper, we follow the QM-Pot method of Sauer and collaborators,[9,10] as implemented in the QMPOT code.[10] The method has been extensively validated in the field of heterogeneous catalysis in zeolites, where it has been used to investigate a number of important properties and the reactivity of both Brønsted acid[25−27] and transition metal sites.[28−31] In the QM-Pot method, the total system (S) is partitioned into two parts, the inner part (I) containing the reaction site and the outer part (O). The interactions within the inner part are treated at the higher computational level, usually full QM. The interactions within the outer part and the interactions between the inner and outer parts are treated at a lower computational level. The lower level can be either a more approximate and, hence, less demanding quantum mechanical method or a parameterized interatomic potential function, Pot. The total energy is partitioned as follows:

$$E_{QM-Pot}(S) = E_{QM}(I) + E_{Pot}(O) + E_{Pot}(I-O) \qquad (1)$$

The interaction term $E_{Pot}(I-O)$ is evaluated using the following relationship:

$$E_{Pot}(I-O) = E_{Pot}(S) - E_{Pot}(O) - E_{Pot}(I) \qquad (2)$$

Equations 1 and 2 together yield the following expression for the total energy:

$$E_{QM-Pot}(S) = E_{QM}(I) + E_{Pot}(S) - E_{Pot}(I) \qquad (3)$$

When bonds are cut across the inner and the outer part in order to define the QM region, the resulting dangling bonds are saturated by "link" (L) atoms. The inner part plus the link atoms form the cluster (C). As a final approximation, when link atoms are present, eq 3 for the total energy is modified to:

$$E_{QM-Pot}(S) = E_{QM}(C) + E_{Pot}(S) - E_{Pot}(C) \qquad (4)$$

Equation 4 has the advantage that link atom contributions are approximately eliminated.[10,32] In most applications the link atoms are hydrogen atoms. In addition, the link atoms are always constrained to be on the original bond that was broken to create the dangling bond. Also, the distance between the link atom and the interior atom to which it is bonded is fixed at a chemically meaningful value. In this study hydrogen atoms that cap a dangling C atom are fixed at 1.07 Å. Tests have shown that the results do not depend strongly on small variations of this value.

Note that the subtraction scheme describes all interactions, including electrostatic terms, between the inner and the outer parts at the potential function level. Hence, the electron density of the embedded cluster differs from the electron density of the free cluster only because of different geometric structures imposed by the embedding force field. Detailed comparison with other QM/MM implementations such as Morokuma's IMOMM approach, which also relies on eq 4, is made in refs 10 and 32.

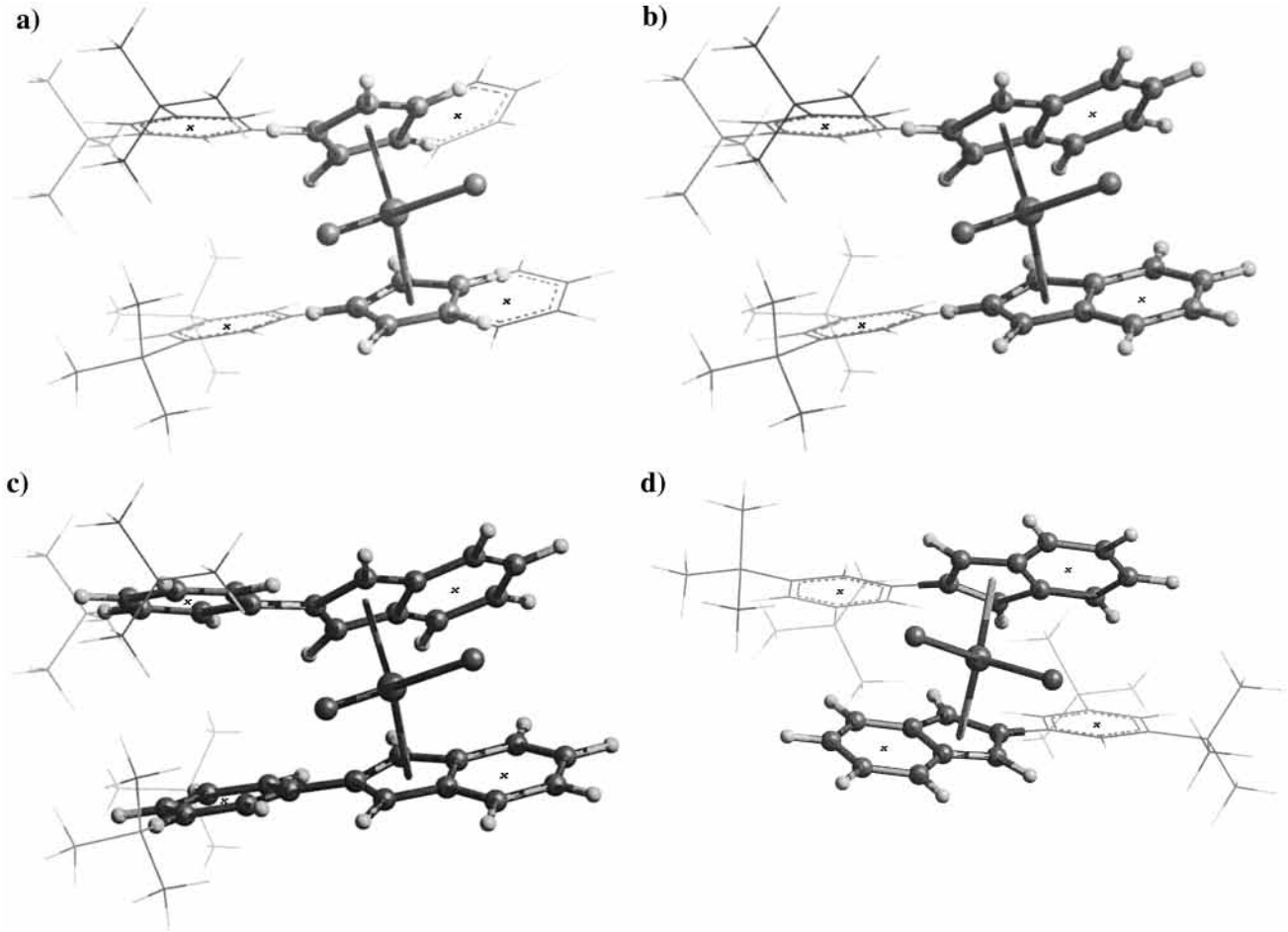

Figure 2. Three possible choices for defining the QM cluster, as illustrated on the tbutyl structure in the meso configuration. Atoms included in the QM cluster are in "ball and stick" representation, while those in the classical host are in "stick" representation. All clusters include the metal center, plus: (a) pentadiene rings (QM1); (b) indenyl rings (QM2); (c) indenyl + phenyl rings (QM3). Link H atoms are explicitly shown. (d) Depicts the QM2 cluster for the rac configuration, clearly showing that for both the interacting phenyl pairs one member belongs to the QM cluster and the other belongs to the classical host.

For the interatomic potential function we use the ESFF force field[33] which is most suitable for metallocene systems and the classical force field calculations are performed with the DISCOVER program.[33] The QM calculations use a density functional (DF) method and are performed using the DMol^3 program.[34,35]

One of the important questions associated with the QM-Pot method is how to define the QM cluster. The answer depends on the system under investigation. For metallocene catalysts the QM part consists of the metal center and atoms in the vicinity, while the rest of catalyst structure, functional groups and polymer fragments away from the metal center are treated at the Pot level. If one wishes to include complete rings in the definition of the cluster, there are three logical choices as shown in Figure 2: (1) QM1, which includes the metal center ($ZrCl_2$) plus the pentadienyl rings; (2) QM2, which includes the metal center plus the two indenyl rings; and (3) QM3, which is the parent structure itself and is a nontrivial cluster for the tbutyl system. For the parent system, using QM3 in a QMPOT calculation is the same as performing a pure QM calculation. The three clusters are in the order of increasing size, consisting of 23, 35, and 55 atoms, respectively. The tbutyl system has 103 atoms.

From a chemical point of view, one would expect that QM1 would be a drastic approximation, because one cuts off the phenyl ring of the indenyl group that involves a fused pentadiene-phenyl pair. A justification for using QM1 can only be provided a posteriori. It is also important to point out that in a typical QM-Pot study of chemical reactions, the surrounding part (treated by Pot) remains nearly unchanged before and after the reaction, i.e., almost all changes take place in the QM cluster. The present application of QM-Pot, on the other hand, is rather unconventional in that most of the changes in going from rac to rotational transition state (TS) to meso occur not near the metallocene core, but rather in the surroundings. This leads to rather unexpected and interesting results as one increases the QM cluster size from QM1 to QM2 to QM3, as we describe in detail in the results section.

Density Functional Calculations. To determine the exchange−correlation functional and the basis set most suitable for the metallocene system of interest, we have compared the computed values of important structural parameters with accurate X-ray diffraction data available for the parent system with methyl groups attached at the (3, 5, 3′, 5′) positions of the phenyl groups.[36] Table 1 summarizes the results for Zr distances from the centers of the two pentadienyl rings (Cp1, Cp2), the Cp1−Zr−Cp2 angle, and the ABCD dihedral angle for various choices of: (1) exchange−correlation functionals, including the nonlocal BP[37] and BOP[38] and local VWN;[39] (2) basis sets, double numeric (DN) and double numeric polarized (DNP); and (3) core states, i.e., all-electron, effective core potential (ECP),[40] and scalar relativity.[34] For numerical basis sets we use a real space cutoff of 4.0 Å, and for numerical integration we use the "medium" grid implemented in DMol^3.[34,35] From extensive

TABLE 1: Comparison of Structural Parameters (Å, deg) for the Zirconocene Parent System of Figure 1 with Methyl Groups in Positions 3, 5, 3′, and 5′

	Zr−Cp1	Zr−Cp2	Cp1−Zr−Cp2	ABCD
experiment[a]	2.240	2.237	130.1	-
ESFF	2.192	2.192	128.5	32.6
BP/dn	2.311	2.313	131.0	33.0
BP/dn/ecp	2.311	2.311	131.0	32.0
BOP/dn	2.376	2.382	131.4	32.0
VWN/dn	2.239	2.233	129.7	32.9
VWN/dn/r[b]	2.232	2.229	129.8	32.8
VWN/dnp/r	2.227	2.225	129.7	32.9

[a] Reference 27. [b] "r" denotes scalar relativistic corrections.

numerical studies we know that as the basis-set cutoff is increased beyond 4.0 Å, the geometry of the optimized structures changes negligibly, and the relative energies do not change by more than 0.2 kcal/mol.[42]

From Table 1, it appears that the local Hamiltonian (VWN) yields a much more accurate structure than the nonlocal choices (BP or BOP), which are designed to correct for typical "overbinding" in local functionals by expanding the ligands outward from the metal center. Even within VWN, the results show a small dependence on the size of the basis set and on whether relativistic effects are included or not. With QM-Pot calculations in mind, it is important to note that ESFF yields an even more contracted and less open structure than VWN. The ESFF distance between Zr and the CP rings are by as much as 0.05 Å shorter than the experimental values, while the DF (VWN/DN) results agree with the latter within better than 0.01 Å. In addition, we have also performed a more detailed analysis of the dependence of energetics on the various choices of exchange−correlation functionals, using geometries generated by both local and nonlocal Hamiltonians.[42] These studies show that using nonlocal functionals on VWN-relaxed geometries do not significantly improve relative energies for the systems/structures considered in this paper. From the above analysis, we decided to consistently use the VWN functional and the DN basis set for the DMol^3 part of our QM-Pot calculations reported below.

4. Description of Ligand Interactions

We expect that an important factor determining the stability of rac and meso conformers is the interaction between the phenyl rings of the zirconocene ligands, both the indenyl part and the phenyl substituent. To investigate how this interaction is described at different computational levels used in QM-Pot calculations, we perform a potential energy (PE) scan for two parallel, sandwich-like benzene molecules located at different distances. Figure 3 shows the PE curves obtained using the DF method and the ESFF force field. In the case of DF calculations with a 4.0 Å cutoff for the basis set (VWN DN/4.0, Figure 3) we made a PE scan up to a separation of 5.0 Å only. To calculate larger separations we use a basis set cutoff of 8.0 Å (VWN DN/8.0, Figure 3). Figure 3 reveals that the basis set cutoff has only a negligible influence on the DF calculated interaction energy for separations smaller than 5.0 Å. For the phenyl rings separated by 5.0 Å, the difference in the interaction energies is less than 0.3 kcal/mol. Much larger differences are found between the DF and ESFF results, the latter method yielding a weaker interaction between the phenyl rings. For two benzene molecules separated by 4.5−5.0 Å, the ESFF force field yields an about 1 kcal/mol lower interaction energy compared to the DF result. It is known that the existing DF functionals, in particular the LDA ones, are unable to describe the London

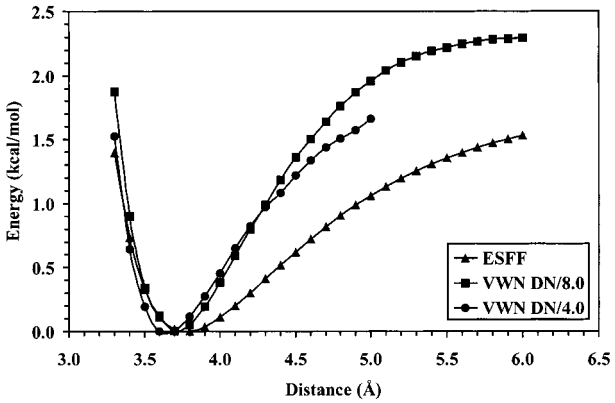

Figure 3. Potential energy curve for two parallel benzene molecules at different separations calculated using DF method and VWN functional and the ESFF force field. The DN/8.0 and DN/4.0 notation indicates the basis set cutoff used in DF calculations.

dispersion properly.[43,44] It is therefore not surprising that the DF calculated stabilization energy for two parallel benzene molecules of 2.02 kcal/mol is actually in worse agreement with the accurate CCSD(T) value of 1.21 kcal/mol, obtained by Hobza et al.,[45] than the ESFF value of 1.83 kcal/mol. Hence, the force field chosen provides a better description of the interaction between the phenyl rings of the zirconocene complex, while the DFT method (VWN) is superior in describing the Zr−cyclopentadiene part. We will see below that hybrid methods such as QM-Pot can take profit from this situation if a proper choice of the QM part is made.

5. Structures

Tables 2 and 3 show important structural parameters for the rac and meso forms of the parent and tbutyl systems and the rotational transition state (TS) structures calculated with the DF method, the QM-Pot method using QM1, QM2, and QM3 cluster models and the ESFF force field alone. The structural parameters include: distances between the Zr atom and the geometrical centers of cyclopentadiene rings (Zr−Cp), distances between geometrical centers of phenyl rings on opposite ligands (Ph_1-Ph_1 and Ph_2-Ph_2), the Cp−Zr−Cp angle, and the ABCD dihedral. As indicated in Figure 1, $Ph_{1(2)}$ refer to all phenyl rings in the system, both within the indenyl rings (hereafter referred to as 5-phenyl) and the phenyl group that is single-bonded to the pentadienyl rings (hereafter referred to as 6-phenyl). In addition, it should be noted that the interacting Ph−Ph pairs for each configuration (rac, meso, and TS) are defined differently and are meant to capture the smallest separations of phenyl rings belonging to opposite ligands. Thus, for rac, both (Ph_1-Ph_1) and (Ph_2-Ph_2) indicate interaction between a 5-phenyl and a 6-phenyl group. For meso, (Ph_1-Ph_1) indicates interaction between two 5-phenyl groups, while (Ph_2-Ph_2) indicates interaction between two 6-phenyl groups. For the TS (Ph_1-Ph_1) indicates interaction between two 5-phenyl groups, whereas (Ph_2-Ph_2) indicates interaction between the close-by pair of 5-phenyl and 6-phenyl groups.

Let us first compare the pure DF and pure ESFF results. As observed for the test system (Table 1) the Zr−Cp distance is too small in all ESFF structures, by more than 0.04 Å as compared to DF structures. This indicates a much stronger Zr−Cp interaction in ESFF than in DF. The Ph−Ph distance, on the other hand, is expanded in the ESFF parent rac structure as compared to DF, indicating a weaker phenyl−phenyl interaction in ESFF. For the parent meso structure, the ESFF 5-phenyl−5-phenyl separation is smaller compared to DF. This, however,

TABLE 2: Important Structural Parameters (Å, deg) of the Parent System[a]

		parameters					
conformation	method	Zr−Cp1	Zr−Cp2	Ph_1-Ph_1	Ph_2-Ph_2[b]	Cp1−Zr−Cp2	ABCD
rac	DF[c]	2.236	2.236	4.74	4.74	129.7	126.9
	QM2	2.250	2.251	5.28	5.28	132.2	113.2
	QM1	2.268	2.268	5.10	5.10	130.5	119.3
	ESFF	2.192	2.192	4.92	4.92	127.8	122.2
meso	DF	2.234	2.237	4.65	4.45	129.7	32.9
	QM2	2.249	2.250	4.61	4.91	130.2	35.0
	QM1	2.265	2.270	4.80	4.71	130.2	35.4
	ESFF	2.192	2.192	4.49	4.61	128.6	33.0
TS	DF	2.233	2.243	5.20	5.33	131.0	70
	QM1	2.270	2.270	5.35	5.39	133.1	77
	ESFF	2.193	2.195	5.19	5.34	134.5	78

[a] See Figure 1 for definitions of the structural parameters. [b] For TS, the Ph_2-Ph_2 column stands for the shorter Ph_1-Ph_2 distance. See text for details. [c] For the parent system, the DF results are the same as QM3 results.

TABLE 3: Important Structural Parameters (Å, deg) of the tbutyl System

		parameters					
conformation	method	Zr−Cp1	Zr−Cp2	Ph_1-Ph_1	Ph_2-Ph_2[a]	Cp1-Zr−Cp2	ABCD
rac	DF	2.238	2.241	4.88	4.94	130.4	117.7
	QM3	2.237	2.237	4.85	4.90	130.1	121.4
	QM2	2.252	2.253	5.10	5.19	132.3	115.5
	QM1	2.268	2.271	5.09	5.15	131.1	115.3
	ESFF	2.192	2.192	4.95	4.99	128.4	115.7
meso	DF	2.234	2.236	4.54	4.81	129.7	29.4
	QM3	2.233	2.236	4.58	5.16	130.2	37.4
	QM2	2.250	2.252	4.50	5.60	130.6	40.8
	QM1	2.268	2.270	4.61	5.05	130.4	30.5
	ESFF	2.192	2.193	4.57	5.17	129.4	30.9
TS	DF	2.234	2.238	5.03	5.15	131.2	71
	QM1	2.268	2.270	5.06	5.43	133.3	76
	ESFF	2.194	2.194	4.92	5.42	134.6	74

[a] For TS, the Ph_2-Ph_2 column stands for the shorter Ph_1-Ph_2 distance. See text for details.

results primarily from the contracted Zr−Cp distance, and the fact that the 5-phenyl rings are fused with the Cp-rings. The Ph_2-Ph_2 distance is more expanded, resulting, as expected, from weaker Ph−Ph interaction in ESFF. For the tbutyl meso structure, the Ph_2-Ph_2 separation is much more expanded than Ph_1-Ph_1, clearly resulting from large steric repulsion of the *tert*-butyl groups, which dominates the much weaker Ph−Ph interaction. This latter repulsion is even more pronounced in ESFF, as evidenced from a much larger Ph_2-Ph_2 separation compared to DF.

Now let us consider the QM-Pot structures. With QM1, the Zr−Cp distances are 0.03 Å more expanded with respect to the DF core, which is already 0.04 Å more expanded than the ESFF core. The Ph−Ph distances are also expanded relative to both DF and ESFF structures. The above can be explained from the fact that in QM1 the overall interactions are weaker than both DF and ESFF. Thus, with respect to ESFF, QM1 has a weaker Zr−Cp interaction, whereas with respect to DF, QM1 has a weaker Ph−Ph interaction.

With QM2, the Zr−Cp separations are closer to full DF result than with QM1, but still about 0.02 Å larger than DF. This causes contraction of ligands compared to QM-Pot results using the QM1 cluster, but expansion compared to the full DF result. For the Ph−Ph separations the QM2 results are worse than QM1, both in parent and tbutyl systems. This is particularly true for the meso conformer, where the two ligands are oriented so that the 5-phenyl rings are on the same side (Figure 2b). This implies that the interactions between these two phenyl rings are described well at the DF level. On the other hand, the interactions between the 6-phenyl rings are still treated at the ESFF level. Tables 2 and 3 show that for the meso structures the distances between centers of the phenyl rings are between 4.5 and 5.6 Å. This is the region where the DF and ESFF methods yield differences in interaction energies of more than 1 kcal/mol (cf. Figure 3). Such unbalanced treatment of interactions between ligands leads to worsening of the structural parameters as compared to a situation wherein all interactions are treated consistently at the DF or ESFF level, for example QM1 and QM3 results. This unbalanced description is even more pronounced in tbutyl than in the parent. Thus, in the tbutyl meso structure, the Ph_1-Ph_1 distance (4.50 Å) is more than 1 Å shorter than the Ph_2-Ph_2 distance (5.60 Å). In full DF and QM1 these distances do not differ by more than 0.5 Å.

The QM3 cluster results for the tbutyl system yield virtually identical Zr−Cp distances as the full DF calculations. This is not surprising, considering that a large part of the interaction between ligands is described well by the DF method. The Ph−Ph distances are also in much better agreement with the DF results, particularly for the rac structure.

As for other structural parameters, QM1 yields results reasonably close to DF for the parent system. The Cp1−Zr−Cp2 angle differs by at most 2°, and the ABCD torsional angle differs by at most 7° for all three stationary points. The QM-Pot calculations using QM1 and QM2 clusters yield similar results for meso for these structural parameters. For the rac form, the QM2 cluster yields an ABCD dihedral angle that is almost 14° smaller than the full DF result. Also the Cp1−Zr−Cp2 angle is in worse agreement with full DF result than QM1 calculations. This again indicates that the QM2 model is not an appropriate choice for the QM-Pot calculations. The ESFF force field yields similar structural parameters to QM-Pot results using the QM1 cluster, although agreement with full QM results is slightly better. The Cp1−ZR−Cp2 angle agrees better than 2° and ABCD dihedral angles better than 5°.

TABLE 4: Relative Energies of the rac and meso Conformers and the Barrier for Rotational Transition (kcal/mol)[a]

energy diff.	method	parent	tbutyl
$E_{meso} - E_{rac}$[a]	DF	1.6	2.8
	QM3	(1.6)	4.0
	QM2	−0.8	0.5
	QM1	0.7	3.2
	ESFF	1.1	3.4
$E_{TS} - E_{rac}$[a]	DF	3.2	6.0
	QM1	3.1	5.4
	ESFF	4.7	2.8

[a] A positive difference indicates that the rac conformer is more stable.

For the tbutyl system the interactions between phenyl rings may not play as important a role as for the parent system. However, the interaction between bulky *tert*-butyl substituents are important. The structural parameter results are similar to those for the parent system. The QM-Pot results for the ABCD dihedral angle with QM2 cluster is slightly smaller compared to the parent system. The QM-Pot results with the QM1 cluster agree better with full DF calculations than for the parent system. For rac and meso conformers, the Cp−Zr−Cp and ABCD dihedral angles agree to within 2.5°. The QM-Pot results with the QM2 cluster for the rac conformer are close to DF and ESFF results. For meso, the structure is much worse due to unbalanced interactions discussed above. The ABCD dihedral angle is overestimated by more than 10°. The QM-Pot results with the QM3 cluster for Cp1−Zr−Cp2 angles are in close agreement with full DF calculations. However, the ABCD torsional angles are too large both for rac and meso conformers. This may point to some mismatch between the DF and ESFF descriptions of interactions between *tert*-butyl groups.

Now, consider the transition state (TS) structures. In pure DF and pure ESFF calculations the transition states are obtained by performing a potential energy surface (PES) scan involving energy minimization for a series of fixed values of the dihedral angle ABCD and locating a maximum in total energy on the PES curve. For QM-Pot calculations, we start with an ESFF TS structure and perform a TS search with QMPOT. Since QM1 appears to be much more consistent than QM2 as compared with full DF structures, and since a QMPOT TS search with QM3 is computationally expensive, we attempted TS searches only with QM1. For both parent and tbutyl systems the structural parameters of rotational transition structures, except the ABCD torsional angle, are similar to the equilibrium rac and meso structures for all computational methods. There are slight changes in the Zr−Cp distances at the full DF level. One of the distances is shorter and one longer than for the rac conformer. The most important structural parameter for the rotational TS is the ABCD torsional angle. For the parent system the QM1 result agrees within 7° with the full DF calculations. The ESFF force field alone yields a slightly worse result within 8°. For the tbutyl system, QM1 calculations give an ABCD angle within 5° and the ESFF force field within 3° of the full DF calculations.

6. Energies

Table 4 shows relative energies of the rac and meso conformers and rotational energy barriers for the parent and tbutyl systems. Comparing the full DF results, it is clear that rac is more stable than meso both in the parent and the tbutyl structures, and the rac stability is even more pronounced in the tbutyl system. This result has strong experimental support if one compares the tacticity of polymers resulting from the BPAmoco catalyst with and without *tert*-butyl groups.[7] The higher stability of rac in the tbutyl system is probably due to the fact that the repelling tbutyl groups are too close to each other in the meso conformation. The ESFF force fieled results are qualitatively similar to the DF results, although ESFF underestimates the rac stability for the parent and overestimates the rac stability for the tbutyl, the latter being perhaps due to a stronger ESFF repulsion between *tert*-butyl groups as compared with DF.

When we compare the above energies to QM-Pot results, it becomes immediately clear that QM1 yields better and more consistent results than QM2, both in the parent and in tbutyl systems. In the parent system, *QM2 incorrectly predicts meso as the more stable structure*. This surprising result arises from the fact that in QM2 the interactions between phenyl rings are treated very differently in rac and meso. In the meso configuration, the (Ph_1-Ph_1) interaction is described well by the DF method, while the (Ph_2-Ph_2) interaction is treated by ESFF. In the rac configuration, on the other hand, both (Ph_1-Ph_1) and (Ph_2-Ph_2) interactions involve one ring treated by DF and the other ring treated by ESFF (Figure 2d). This means that the Ph−Ph interaction is actually a part of the E_{Pot}(I−O) interaction (see eq 2) and is therefore treated classically by means of ESFF. The above, coupled with the fact that Ph−Ph interactions in DF can lead to more than a kcal/mol energy gain with respect to ESFF (see Figure 3), would seem to explain why the meso structure is predicted to be more stable than rac in QMPOT calculations with QM2. The enhanced meso stability with QM2 would also explain why the rac structure is only 0.5 kcal/mol more stable than meso in the tbutyl system. QM1, on the other hand, yields energetics in much better agreement with full DF results and correctly predicts an enhanced rac stability for the tbutyl system. QM3, as expected, also predicts a reasonable rac−meso energy difference for the tbutyl system.

For pure rac and meso structures, ESFF energies are in reasonably good agreement with DF results. However, they are not as good for rotational transition barriers compared with QM1. One can see from Table 3 that the ESFF TS geometry for the parent consists of a tight Zr−Cp distance, just as in rac or meso. However, the real difference arises in the Ph−Ph distances, which for the ESFF parent structure is almost the same as for the DF structure, whereas for ESFF the rac geometry is more expanded with respect to the DF geometry. This leads to a higher ESFF rotational barrier for the parent system. The situation is reversed in the tbutyl system, leading to a lower barrier compared with DF. QM1, on the other hand, yields more consistent expanded structures, in rac, meso, and TS, and the barrier heights are in closer agreement with DF.

7. Summary and Discussion

Of the three different QM clusters chosen, the smallest one, i.e., QM1 yields the most consistent relative energetics of rac, meso and TS configurations, both in the parent and the tbutyl systems. QM1 correctly predicts: (1) rac as the more stable rotamer; (2) the increased relative stability of rac in the tbutyl system; (3) the increased TS barrier for the tbutyl system. QM2 incorrectly predicts meso to be more stable in the parent structure and predicts a rac-meso energy difference that is too small for the tbutyl system. QM3 results are much better than QM2 (for the tbutyl system) but not necessarily better than QM1, even though QM3 requires a much higher computational cost.

It is difficult to pinpoint an exact cause for the superiority of QM1 in the computation of reaction barriers. It can probably

be attributed to ESFF not being parameterized well for the local environment arising at the TS dihedral angle and QM1 making amends for it by treating the strong interactions at the metal center correctly in a DF manner.

One may argue that in the absence of experimental data for the meso−rac energy difference and the rotational barrier we do not really know if the DF (and QM1) results are superior to the ESFF results. However, the better description of the Zr−cyclopentadiene interaction by DFT as evidenced by the better distance compared to experimental values (Table 1) is a strong hint. Moreover, the biggest justification of using a hybrid QM/MM approach as opposed to a pure force field calculation comes in the future computations of reaction barriers for the polymerization step. Such processes where one makes or breaks chemical bonds are notoriously difficult to treat for any type of force field.

As a first application of the QM-Pot method to metallocene catalysis, we have uncovered that one needs to be cautious in the definition of the QM cluster. Any practical force field always has small structural and energetic differences with first-principles (DF) results. Unless these differences are treated in a consistent manner, one could get poorer results with QM/MM calculations than even with a pure force field method. In our particular example, several interactions play an important role in determining the final structure and energetics: the interaction between negatively charged pentadiene rings and the Zr center and interactions between two pairs of phenyl rings. In QM1 and QM3 the interactions are treated consistently, which unfortunately is not the case in QM2 by its very construction.

With future applications for polymerization reactions in mind, it should be added that the present application was complicated by the fact that the rac, meso, and TS geometries have significant differences in the configuration of the ligands that are typically described by classical force fields. This is different from a conventional QM-Pot application in which most changes take place (in the form of a chemical reaction) within the QM cluster, and not in the classical surrounding. Thus, all of the problems regarding the inconsistencies of QM2 between rac and meso would probably not arise if one is studying polymerization in a bridged zirconocene catalyst, for which the catalyst is not free to rotate. Nevertheless, it is encouraging to see that even a small cluster such as QM1 is able to yield accurate energetics consistently for all of the configurations. With relatively small computational requirements, this should open the door for many more applications soon.

References and Notes

(1) Gates, B. C. *Catalytic Chemistry*; John Wiley & Sons: New York, 1992; p 102.

(2) Crabtree, R. H. *The Organometallic Chemistry of the Transition Metals*; John Wiley & Sons: New York, 1988; p 267.

(3) Spaleck, W.; Kuber, F.; Winter, A.; Rohrmann, J.; Bachmann, B.; Antberg, M.; Dolle, V.; Paulus, E. F. *Organometallics* **1994**, *13*, 954.

(4) Spaleck, W.; Aulbach, M.; Bachmann, B.; Kuber, F.; Winter, A. *Macromol. Symp.* **1995**, *89*, 237.

(5) Toto, M.; Cavallo, L.; Corrandini, P.; Moscardi, G.; Resconi, L.; Guerra, G. *Macromolecules* **1998**, *31*, 3431.

(6) Coates, G. W.; Waymouth, R. M. *Science* **1995**, *267*, 217.

(7) Golab, J. *CHEMTECH*, April **1998**, 17.

(8) Maciejewski-Petoff, J. L.; Agoston, T.; Lal, T. K.; Waymouth, R. M. *J. Am. Chem. Soc.* **1998**, *120*, 11316.

(9) Eichler, U.; Kölmel, C. M.; Sauer, J. *J. Comput. Chem.* **1997**, *18*, 463.

(10) Sierka, M.; Sauer, J. *J. Chem. Phys.* **2000**, *112*, 6983.

(11) Warshel, A.; Levitt, M. *J. Mol. Biol.* **1976**, *103*, 227.

(12) Singh, U. C.; Kollman, P. A. *J. Comput. Chem.* **1986**, *7*, 718.

(13) Field, M. J.; Bash, P. A.; Karplus, M. *J. Comput. Chem.* **1990**, *11*, 700.

(14) Stanton, R. V.; Hartsough, D. S.; Merz, K. M., Jr. *J. Phys. Chem.* **1993**, *97*, 11868.

(15) Maseras, F.; Morokuma, K. *J. Comput. Chem.* **1995**, *16*, 1170.

(16) Bakowies, D.; Thiel, W. *J. Phys. Chem.* **1996**, *100*, 10580.

(17) Amara, P.; Field, M. J. In *Encyclopedia of Computational Chemistry*; Schleyer, P. v. R., Allinger, N. L., Kollman, P. A., Clark, T., Schaefer, H. F., III, Gasteiger, J.; Schreiner, P. R., Eds.; Wiley: Chichester, 1998; Vol. 1, p 431.

(18) Ruiz-López, M. F.; Rivail, J.-L. In *Encyclopedia of Computational Chemistry*; Schleyer, P. v. R., Allinger, N. L., Kollman, P. A., Clark, T., Schaefer, H. F., III, Gasteiger, J., Schreiner, P. R., Eds.; Wiley: Chichester, 1998; Vol. 1, 437.

(19) Froese R. D. J.; Morokuma, K. In *Encyclopedia of Computational Chemistry*; Schleyer, P. v. R., Allinger, N. L., Kollman, P. A., Clark, T., Schaefer, H. F., III, Gasteiger, J., Schreiner, P. R., Eds.; Wiley: Chichester, **1998**; Vol. 2, p 1244.

(20) Gao, J. In *Encyclopedia of Computational Chemistry*; Schleyer, P. v. R., Allinger, N. L., Kollman, P. A., Clark, T., Schaefer, H. F., III, Gasteiger, J., Schreiner, P. R., Eds.; Wiley: Chichester, 1998; Vol. 2, p 1257.

(21) Merz, K. M., Jr.; Stanton, R. V. In *Encyclopedia of Computational Chemistry*; Schleyer, P. v. R., Allinger, N. L., Kollman, P. A., Clark, T., Schaefer, H. F., III, Gasteiger, J., Schreiner, P. R., Eds.; Eds.; Wiley: Chichester, 1998; Vol. 4, p 2330.

(22) Woo, T. K.; Margl, P. M.; Deng, L.; Cavallo, L.; Ziegler, T. *Catal. Today* **1999**, *50*, 479.

(23) Woo, T. K.; Margl, P. M.; Blöchl, P. E.; Ziegler, T. *J. Phys. Chem. B* **1997**, *101*, 7877.

(24) Yoshida, T.; Koga, N.; Morokuma, K. *Organometallics* **1996**, *15*, 766.

(25) Eichler, U.; Brändle, M.; Sauer, J. *J. Phys. Chem. B* **1997**, *101*, 10035.

(26) Brändle, M.; Sauer, J. *J. Am. Chem. Soc.* **1998**, *120*, 1556.

(27) Sierka, M.; Eichler, U.; Datka, J.; Sauer, J. *J. Phys. Chem. B* **1998**, *102*, 6397.

(28) Rodriguez-Santiago, L.; Sierka, M.; Branchadell, V.; Sodupe, M.; Sauer, J. *J. Am. Chem. Soc.* **1998**, *120*, 1545.

(29) Nachtigallová, D.; Nachtigall, P.; Sierka, M.; Sauer, J. *Phys. Chem. Chem. Phys.* **1999**, *1*, 2019.

(30) Ricchiardi, G.; de Man, A. J. M.; Sauer, J. *Phys. Chem. Chem. Phys.* **2000**, *2*, 2195.

(31) Nachtigall, P.; Nachtigallová, D.; Sauer, J. *J. Phys. Chem. B* **2000**, *104*, 1738.

(32) Sauer, J.; Sierka, M.; *J. Comput. Chem*., in print.

(33) Discover 2.9.8/96.0/4.0.0 User Guide Part I, MSI, San Diego, September 1996. For ESFF ForceField, see Pages 63−74.

(34) Delley, B. *J. Chem. Phys.* **1990**, *92*, 508; *J. Phys. Chem.* **1996**, *100*, 6107.

(35) Delley, B. *Int. J. Quantum Chem.* **1998**, *69*, 423.

(36) Hauptman, E.; Waymouth, R. M.; Ziller, R. M. *J. Am. Chem. Soc.* **1995**, *117*, 11586.

(37) Becke, A. D. *Phys. Rev. A* **1988**, *38*, 3098; Perdew, J. P.; Wang, Y. *Phys. Rev. B* **1992**, *45*, 13244.

(38) Tsuneda, T.; Suzumura, T.; Hirao, K. *J. Chem. Phys.* **1999**, *110*, 10664.

(39) Vosko, S. H.; Wilk, L.; Nusair, M. *Can. J. Phys.* **1980**, *58*, 1200.

(40) Dolg, M.; Wedig, U.; Stoll, H.; Preuss, H. *J. Chem. Phys*. **1997**, *86*, 866.

(41) MSI online documentation for $DMol^3$ in Cerius2_4.0 at: http://www.msi.com/doc/cerius40/quantum/3a_DMol3.html#605951.

(42) Andzelm, J. et al., in preparation.

(43) Kristian, S.; Pulay, P. *Chem. Phys. Lett.* **1994**, *175*, 229.

(44) Hobza, P.; Šponer, J.; Reschel, T. *J. Comput. Chem.* **1995**, *11*, 1315.

(45) Hobza, P.; Selzle, H. L.; Schlag, E. W. *J. Phys. Chem.* **1996**, *100*, 18790.